Memo version

BESIII Analysis Memo

February 27, 2019

Study of $e^+ e^- \to \phi(1020)\, \pi^+ \pi^-$

Y. X. Tan[a], Y. K. Sun[a], Y. T. Zhang[a], W. B. Yan[a], and G. S. Huang[a]

[a]*University of Science and Technology of China*

Internal Referee Committee

Abstract

Using data samples collected with the BESIII detector operating at the Beijing Electron Positron Collider, we study $e^+e^- \to \phi(1020)\, \pi^+ \pi^-$ at 19 center-of-mass energies from 2.0 to 3.08 GeV. The Born cross sections are measured at each energy point and are found to agree well with previous results. A structure around $\sqrt{s} = 2.1$ GeV/c^2, corresponding to the so called $Y(2175)$, is observed in the cross section line shape of $e^+e^- \to \phi(1020)\, \pi^+ \pi^-$. A fit to the line shape results in a mass of $(2113 \pm 5 \pm 10)$ MeV/c^2 and a width of $(109 \pm 11 \pm 10)$ MeV/c^2, where the first error is statistical and the second is systematic.

Contents

1 Introduction

The observation of $\phi(2170)$ was first reported by the BABAR Collaboration in the initial-state-radiation (ISR) process $e^+e^- \to \phi(1020)f_0(890)$ [1], with mass $m = 2.175 \pm 0.010 \pm 0.015\ GeV/c^2$ and width $\Gamma = 58 \pm 16 \pm 20\ MeV$. It was later confirmed by BES Collaboration in the $\phi(1020)f_0(890)$ invariant mass spectrum of $J/\psi \to \eta\phi(1020)f_0(890)$ decays [2] and by Belle Collaboration via the same ISR process [3]. The Particle Data Group (PDG) assigns all these observations to a new state refereed to as the $\phi(2170)$. BESIII updated it by using $J/\psi \to \eta\phi f_0(980)$ [4] and $e^+e^- \to \eta\phi f_0(890)$ at center-of mass energy between 3.7 to 4.6 GeV [5].

Since the $\phi(2170)$ resonance is produced via ISR in e^+e^- collision, its $J^{PC} = 1^{--}$. This observation stimulated the theoretical speculation that $\phi(2170)$ may be an s-quark counterpart of the $Y(4260)$ since both are produced in e^+e^- annihilation and exhibit similar decay patterns [6]. Many interpretations have been proposed for the $\phi(2170)$, which are consistent with the experimental measured masses within errors. These interpretations include a traditional $s\bar{s}$ state [7, 8, 9], an $s\bar{s}g$ hybrid [6, 7], a tetraquark state [10, 11, 12], a $\Lambda\bar{\Lambda}$ bound state [13, 14, 15] and an ordinary $\phi(1020)$ $f_0(980)$ resonance produced by interactions between the final particles [16, 17].

In this memo, we present a study of $e^+e^- \to \phi(1020)\ \pi^+\ \pi^-$ at 19 energies from 2.0 to 3.08 GeV.

2 A Brief Description of BEPCII and BESIII

BEPCII [18] is a double-ring e^+e^- collider designed to provide a peak luminosity of $10^{33}\ \ \mathrm{cm}^{-2}s^{-1}$ at the center of mass energy of 3770 MeV. The BESIII [18] detector has a geometrical acceptance of 93% of 4π and has four main components: (1) A small-cell, helium-based (40% He, 60% C_3H_8) main drift chamber (MDC) with 43 layers providing an average single-hit resolution of 135 μm, and a charged-particle momentum resolution in a 1 T magnetic field of 0.5% at 1 GeV/c. (2) An electromagnetic calorimeter (EMC) consisting of 6240 CsI(Tl) crystals in a cylindrical structure (barrel) and two endcaps. The energy resolution at 1.0 GeV/c is 2.5% (5%) in the barrel (endcaps), and the position resolution is 6 mm (9 mm) in the barrel (endcaps). (3) Particle Identification is provided by a time-of-flight system (TOF) constructed of 5-cm-thick plastic scintillators, with 176 detectors of 2.4 m length in two layers in the barrel and 96 fan-shaped detectors in the endcaps. The barrel (endcap) time resolution of 80 ps (110 ps) provides 2σ K/π separation for momenta up to $\sim$ 1.0 GeV/c. (4) The muon system (MUC) consists of 1000 m^2 of Resistive Plate Chambers (RPCs) in nine barrel and eight endcap layers and provides 2 cm position resolution.

3 Data Samples and Monte Carlo simulation

3.1 Data Samples

This analysis is performed under the framework of the BOSS665. The data samples used for this analysis are the high luminosity R-scan data collected in 2015 combined with a dedicated set of e^+e^- collision data at 2.125GeV(summarized in Table 1)[19]. The luminosity is measured using Bhabha events.

Table 1: Data samples used in this analysis.

$\sqrt{s}$ GeV	Luminosity (pb^{-1})	Run Number
3.080	126.183	39355-39618
3.020	17.262	39711-39738
3.000	15.863	39680-39710
2.981	16.056	39651-39679
2.950	15.949	39619-39650
2.900	105.015	39775-40069
2.800	1.009	40440-40443
2.700	1.034	40436-40439
2.6464	34.017	40300-40435
2.6444	33.585	40128-40298
2.500	1.098	40771-40776
2.396	66.817	40436-40769
2.3864	22.557	40806-40951
2.3094	22.070	41240-41411
2.2324	11.845	41123-41239
2.200	13.678	40989-41121
2.175	10.591	41416-41532
2.150	2.847	41533-41570
2.125	108.49	42004-43253
2.100	12.150	41588-41728
2.050	3.352	41911-41957
2.000	10.121	41729-41909

3.2 Monte Carlo simulation

Monte-Carlo (MC) samples simulated with the full detector are used to determine the detection efficiency of signals, optimize event selection criteria, and estimate backgrounds. The simulation program provides an event generator, contains the detector geometry description, and simulates the detector response and signal digitization. The detector geometry, material description and the transportation of the decay particles through the detector including interactions are handled by GEANT4.

We also generate 100 K MC sample for following each channel by ConExc generator to study selection efficiency and optimize selection criteria as listed in Table 2.

Table 2: Exclusive MC samples.

Decay Mode	Generator Model	Reference
$e^+e^- \to \phi(1020)\,\pi^+\,\pi^-$	PHSP	PHSP
$e^+e^- \to \phi(1020)\,f_0(980)$	PHSP	PHSP

4 Analysis of $e^+e^- \to \phi(1020)\,\pi^+\,\pi^-$ at $\sqrt{s}$ = 2.125 GeV

4.1 Event Selection

For decay channel of interest $e^+e^- \to \phi(1020)\,\pi^+\,\pi^-$, the $\phi(1020)$ candidate is reconstructed with $K^+\,K^-$. The following event selection criteria are applied to both data and MC samples:

- Each charged track is required to be well reconstructed from hits in the MDC. They are required to originate from the interaction region: $V_r = \sqrt{V_x^2 + V_y^2} < 1.0$ cm and $|V_z| < 10.0$ cm. The charged tracks must be within the polar angle $|\cos\theta| < 0.93$. The number of good charged tracks which satisfy above selection criteria is required to be 3 or 4, and the net charge restricted to be 0 when the number of good charged tracks is 4.

- The combined information of TOF and dE/dx are used to calculate probabilities for each charged track $Prob_{PID}(i)$ for the hypotheses that a track is a pion, kaon or proton, where i ($i = \pi/K/p$) is the particle type. For pion candidates, we require $Prob_{PID}(\pi) > Prob_{PID}(K)$ and $Prob_{PID}(\pi) > Prob_{PID}(p)$ and $N_{\pi^+} = N_{\pi^-} = 1$. For kaon candidates, we assumed the rest charged particles are all kaons.

- In order to reconstruct the primary vertex, vertex fitting with the $K^\pm\pi^+\pi^-$ is applied.

- One-constraint (1C) kinematic fit is applied under the hypothesis of $e^+e^- \to K^+\,K^-\,\pi^+\,\pi^-$, where K^+ or K^- is treated as a missing particle with mass of 0.4937 GeV/c^2. For events with two identified Kaon candidates (one K^+ and one K^-), two possible cases will be tried and the combination with smaller χ^2_{1C} is used in further analysis. The distribution of χ^2_{1C} is displayed in Figure 1 (a) and the χ^2_{1C} is required to be less than 10.

- In the end, for particles assumed as kaon above, we require $Prob_{PID}(K) > Prob_{PID}(\pi)$ and $Prob_{PID}(K) > Prob_{PID}(p)$ and at least one Kaon is identified.

After above selection criteria applied, the invariant mass distribution of K^+K^- is shown in Figure 1 (b). The $\phi(1020)$ signal is observed significantly.

4.2 Background study

4.2.1 Backgrounds study from inclusive MC sample

The inclusive MC events generated at $\sqrt{s}$ = 3.080 GeV with different processes are employed to check the potential background contamination. The inclusive events includes hadronic events and QED events.

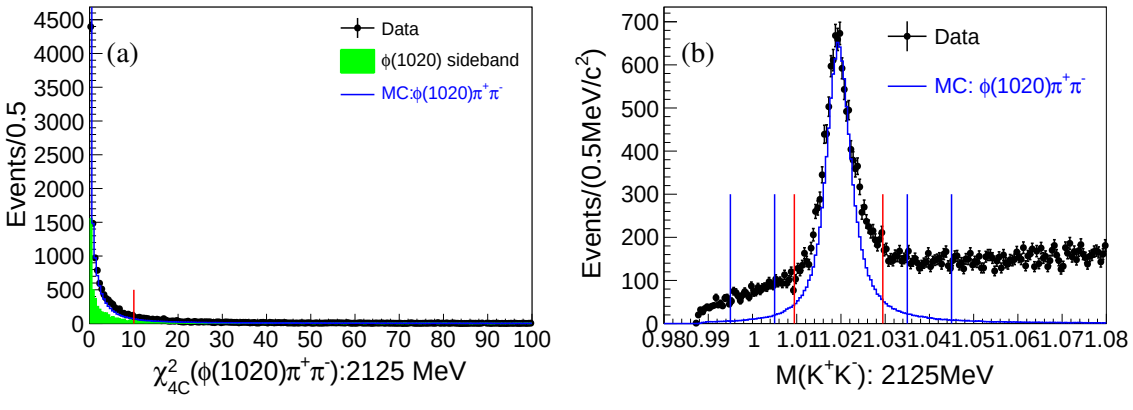

Figure 1: (a) $\chi^2_{1C}(\phi(1020)\,\pi^+\,\pi^-)$ distributions: the black dots with error are experimental data events in $\phi(1020)$ signal region, green histogram is events in $\phi(1020)$ sideband regions and blue histogram is from phase space MC sample $e^+e^- \to \phi(1020)\,\pi^+\,\pi^-$. (b) M($K^+K^-$) distributions: the black dots with error are experimental data events and blue histogram is from phase space MC sample $e^+e^- \to \phi(1020)\,\pi^+\,\pi^-$.

By applying the same selection criteria on inclusive MC sample, the main backgrounds are found to be $e^+e^- \to K^\star(892)^0\,K^-\,\pi^-\,+\,c.c.$, $e^+e^- \to K_2^\star(1430)^0\,K^-\,\pi^-\,+\,c.c.$, $e^+e^- \to K_1(1270)^+\,\pi^-\,+\,c.c.$, $e^+e^- \to K_1(1410)^+\,\pi^-\,+\,c.c.$ and $e^+e^- \to K^+\,K^-\,\rho^0$.

4.2.2 Backgrounds study with exclusive MC samples

With ConExc generator, we generated 100K MC sample for each mode of $e^+e^- \to K^+\,K^-\,\rho^0$, $e^+e^- \to K^\star(892)^0\,K^-\,\pi^-\,+\,c.c.$, $e^+e^- \to K_1(1270)^+\,\pi^-\,+\,c.c.$, $e^+e^- \to K_1(1410)^+\,\pi^-\,+\,c.c.$ and $e^+e^- \to K_2^\star(1430)^0\,K^-\,\pi^-\,+\,c.c.$. By applying the same selection criteria on these exclusive MC samples, the corresponding distributions of M(K^+K^-) are shown in Figure 2.

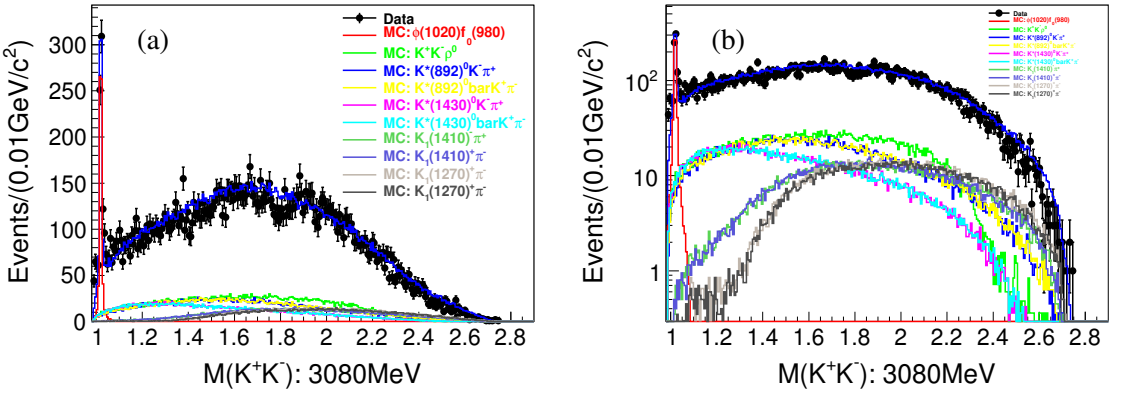

Figure 2: Comparison between Data and MC samples on M(K^+K^-) distribution.

4.3 Partial wave analysis

To obtain the contribution from the possible intermediate state, for example the $f_0(980)$ and σ, to describe the ϕ-background events. We use the Partial Wave Analysis method by unbinned maximum likelihood fitting. The non-ϕ background events are described with the ϕ sidebands as described above. In PWA, signal events in the ϕ signal sideband are given positive weight in log likelihood and the sideband events are given negative weight to cancel background in the data sample. Amplitudes are fitted to relativistic tensor expressions which are documented in Ref.[20]. In the PWA, the $e^+e^- \to \phi\pi^+\pi^-$ process is well described by four subprocesses: $e^+e^- \to f_0(980), \sigma, f_0(1370), f_2(1270)$. σ is described with the form used fitting $\pi\pi$ elastic scattering data [21], $f_0(980)$ is described with a Flatte formula [22], and others are described with relativistic Breit-Winger (BW) function. The resonance parameters are fixed on the values determined in previous BES analysis on $J/\psi \to \phi\pi\pi$ and $J/\psi \to \omega\pi\pi$ [23, 24].(Detailed information please seen in Appendix A).

4.4 Comparison of MC and Data

A comparison of the data and fitting results include both on the mass and angular distributions, shown in Figure 3, Figure 4 and Figure 5, indicate that the present PWA model could describe data well.

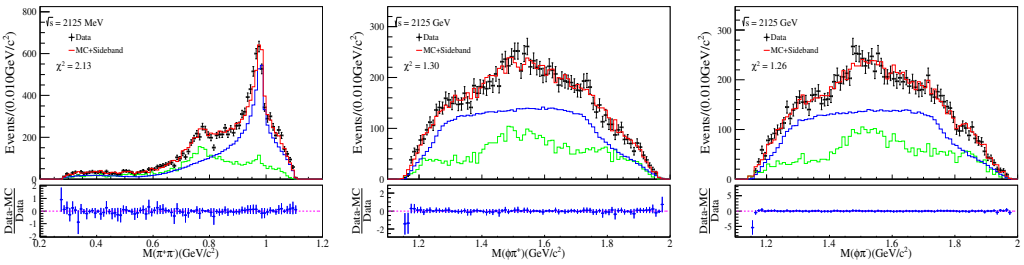

Figure 3: Comparison between Data and MC samples on mass distribution.

4.5 Signal extraction

The number of signal events $e^+e^- \to \phi(1020)\pi^+\pi^-$ is obtained by fitting on the K^+K^- invariant mass spectrum within region [0.98, 1.09] GeV/c^2. The unbinned maximum likelihood method is performed. The fitting PDF is described with the sum of signal (P-wave BW convoluted with Gaussian function) and background (Argus function) contributions.

The fitting results are shown in Figure 6. The number of signal events are obtained to be 9372.1 ± 144.7, the parameters of Gaussian function are obtained to be M = -0.06 MeV and σ = 1.8 MeV, and the goodness of the fit is χ^2/ndf = 1.93.

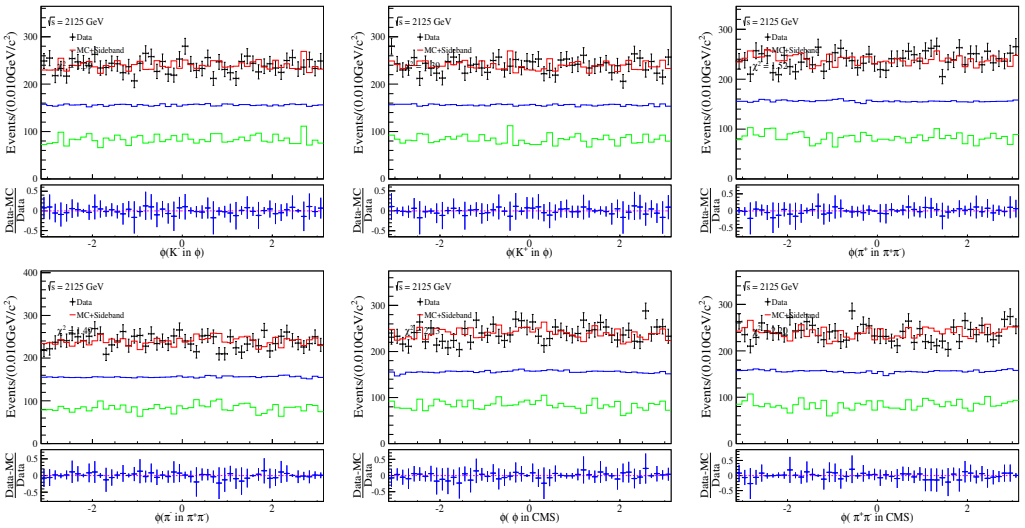

Figure 4: Comparison between Data and MC samples on ϕ *angle distribution*.

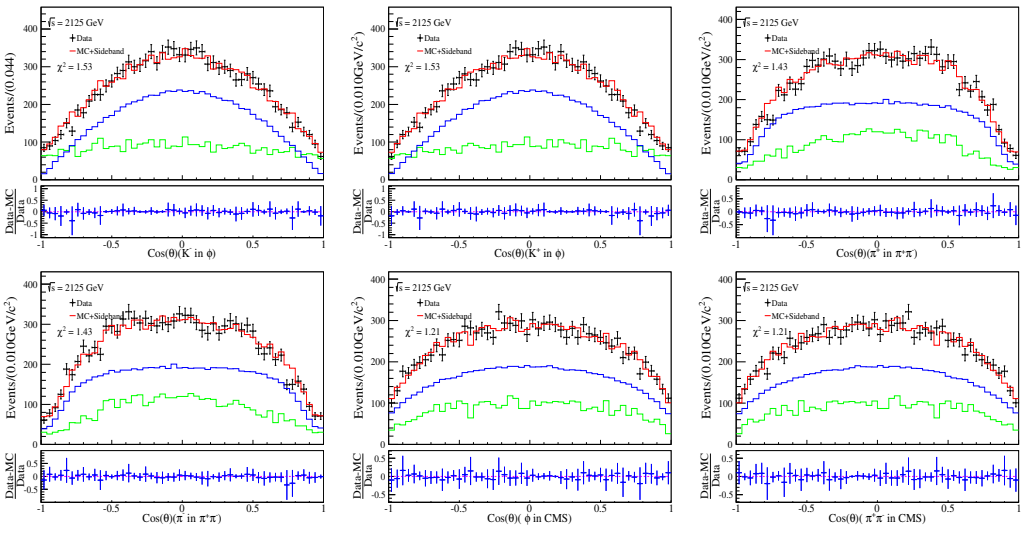

Figure 5: Comparison between Data and MC samples on Cos(θ) *distribution*.

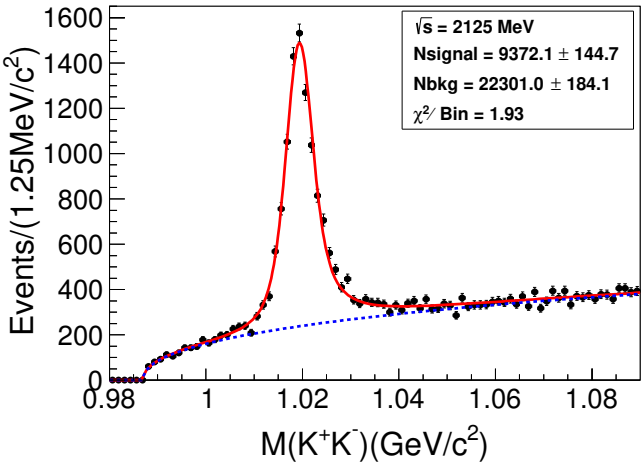

Figure 6: Fit of M(K^+K^-) distribution: Signal is described by P-wave BW convoluted with Gaussian function, and background is described by Argus function.

4.6 Cross section measurement

The Born cross section is calculated by:

$$\sigma(e^+e^- \to \phi\pi^+\pi^-) = \frac{N^{obs}}{\mathcal{L}_{int} \cdot (1+\delta^r) \cdot (1+\delta^v) \cdot \epsilon \cdot \mathcal{B}}, \quad (1)$$

where N^{obs} is the number of observed signal events, $\mathcal{L}_{int}$ is the integrated luminosity, $(1+\delta^r)$ is the ISR correction factor which is obtained by QED calculation and taking the line shape of the Born cross section measured by the BABAR experiment. $(1+\delta^v)$ is the vacuum polarization (VP) factor which is taken from QED calculation with an accuracy of 0.5%, ϵ is the detection efficiency including reconstruction and all selection criteria, $\mathcal{B}$ is the product branching ratio, $\mathcal{B}(\phi(1020) \to K^+K^-)$, taken from the Particle Data Group (PDG).

The final selection efficiency is measured to be 40.53% according to MC simulation. The measured Born cross section for $e^+e^- \to \phi(1020)\,\pi^+\pi^-$ is (431.6 ± 6.7) pb. Here the error is statistical only.

4.7 Systematic error estimation

Systematic errors in the cross section measurement come from the luminosity measurement, tracking efficiency, PID efficiency, kinematic fit, background and fittingrange estimation, radiative correction and branching fraction of $\phi(1020) \to K^+K^-$.

The integrated luminosity of this data sample was measured using large angle Bhabha events, and has an estimated uncertainty of 1.0%.

The tracking efficiency uncertainty is estimated to be 1.5% for each track from a study of the control sample $e^+e^- \to K^0_s K^\pm \pi^\mp$ [25]. So 4.5% is taken as the systematic uncertainty on tracking efficiency.

The PID efficiency uncertainty is estimated to be 1.0% $for\ \pi^\pm$ and 1.5% $for\ K^\pm$ from a study of the control sample $e^+e^- \to K^0_s K^\pm \pi^\mp$ [25]. So 3.5% is taken as the systematic uncertainty on PID efficiency.

The uncertainty from the kinematic fit comes from the inconsistency between the data and MC simulation of the helix parameters. Following the procedure described in Ref[20], we take the difference between the efficiencies with and without the helix parameters correction as the systematic error, which is 1.0%.

Uncertainties due to the choice of background shape and fitting range are estimated by varying the background function from Argus function to second-order polynomial and by extending the fit range.

Uncertainties in the initial cross section line shape used in generator introduce systematic uncertainties in the radiative correction factor and the efficiency. This is estimated using different line shape measured by BABAR and Belle. The difference in $(1+\delta)\times\epsilon$ is 1.0%.

The uncertainty in $\mathcal{B}(\phi(1020) \to K^+K^-)$ is 1.3% from PDG2018.

The trigger simulation, the event start time determination, and the final-state-radiation simulation are well understood; the total systematic error due to these sources is estimated to be less than 1.0%.

Table 3 summarize all the systematic error sources and their contributions. Assuming all the systematic uncertainty sources are independent, the total systematic error is 7.4%.

Table 3: Summary of systematic uncertainties (%) in the cross section measurement of $e^+e^- \to \phi(1020)\pi^+\pi^-$.

Source	Value
Luminosity	1.0
Tracking	4.5
PID	3.5
Kinematic fit	3.8
Fitting range	0.3
Signal shape	2.1
Background shape	7.0
ISR factor	0.2
Branching fraction	1.3
Others	1.0
Sum	7.4

5 Analysis of $e^+e^- \to \phi(1020)\,\pi^+\,\pi^-$ at other energy points

The same event selection criteria are implemented on the other data samples taken at different CM energies in Table 1. Except for 3 energy points: 2.500GeV, 2.700GeV and 2.800GeV, since the luminosity at the three points too low to select enough signal data for the PWA .

5.1 Signal extraction

The number of signal events $e^+e^- \to \phi(1020)\,\pi^+\pi^-$ is obtained by fitting on the K^+K^- invariant mass spectrum within region [0.98, 1.09] GeV/c^2. The unbinned maximum likelihood method is performed. The fitting PDF is described with the sum of signal (P-wave BW convoluted with Gaussian function) and background (Argus function) contributions.

The fitting results are shown in Figure 7 and 8.

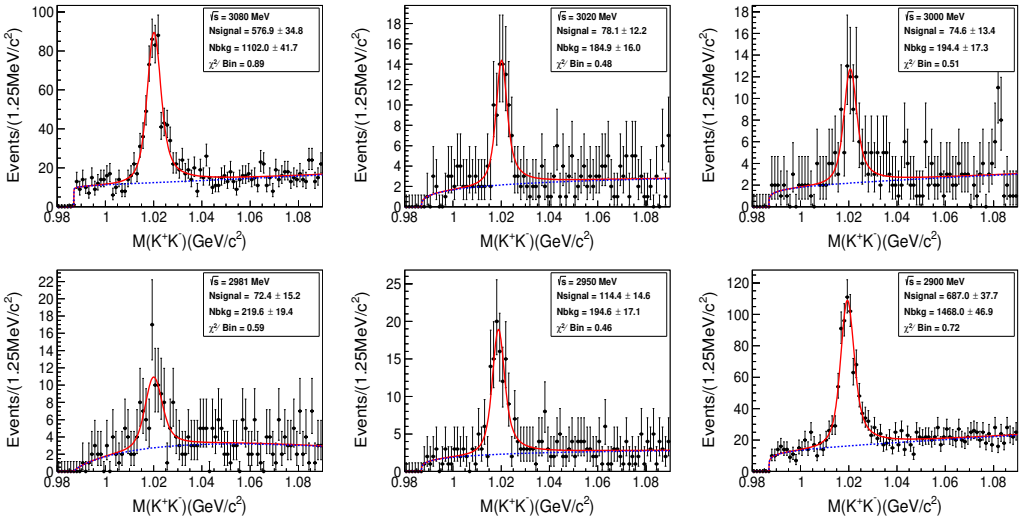

Figure 7: Comparison between Data and MC samples on M(K^+K^-) distribution.

5.2 Comparison between data and MC from PWA method

These plots display the invariant mass, ϕ angle and $Cos(\theta)$ distribution of $\pi^+\pi^-$. The good agreement on these projections indicate that our MC samples produced from PWA can describe the data well, hence we can use these MC samples to estimate the efficiency of data.

5.3 Cross section measurement

The Born cross section is calculated by:

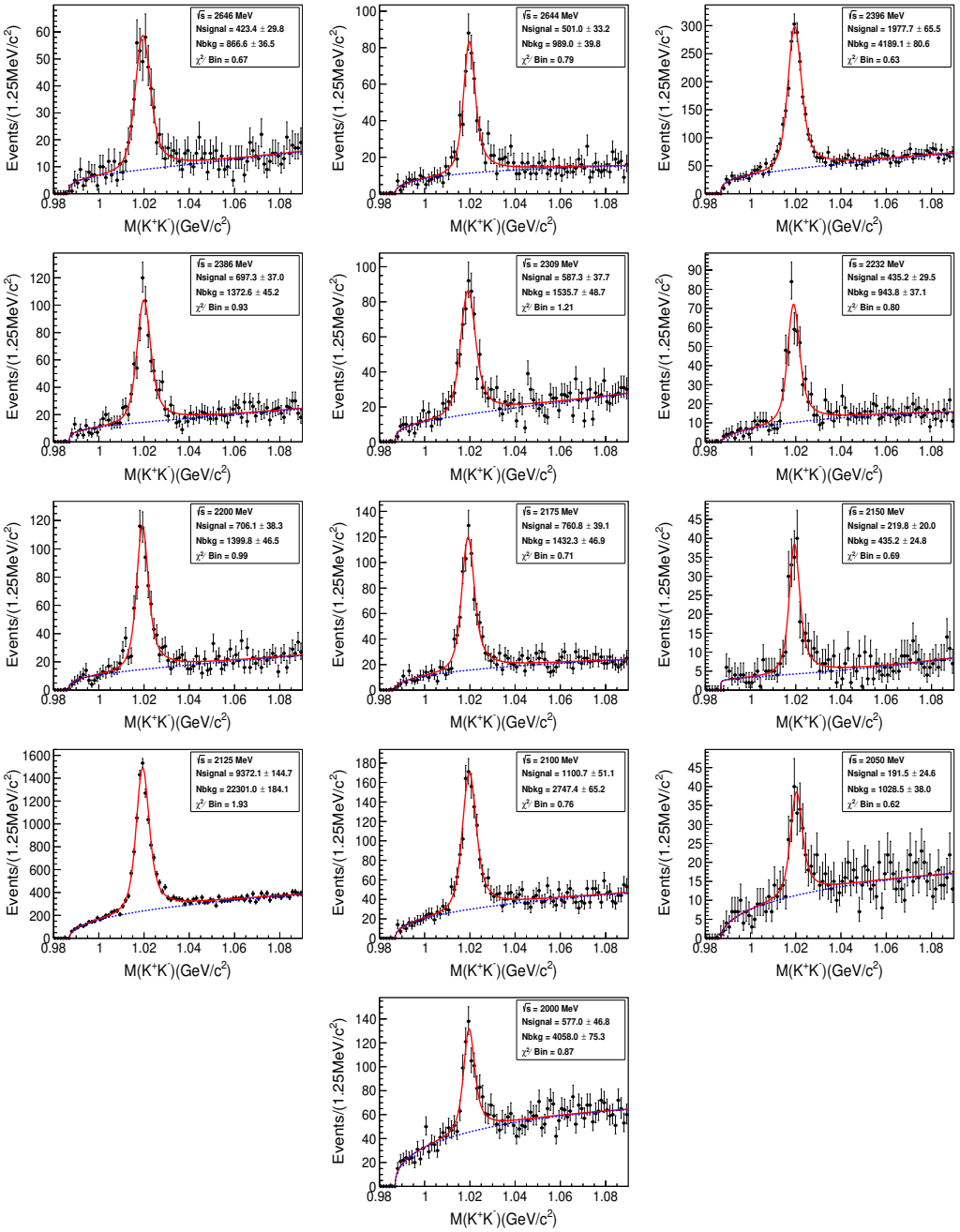

Figure 8: Comparison between Data and MC samples on M(K^+K^-) distribution.

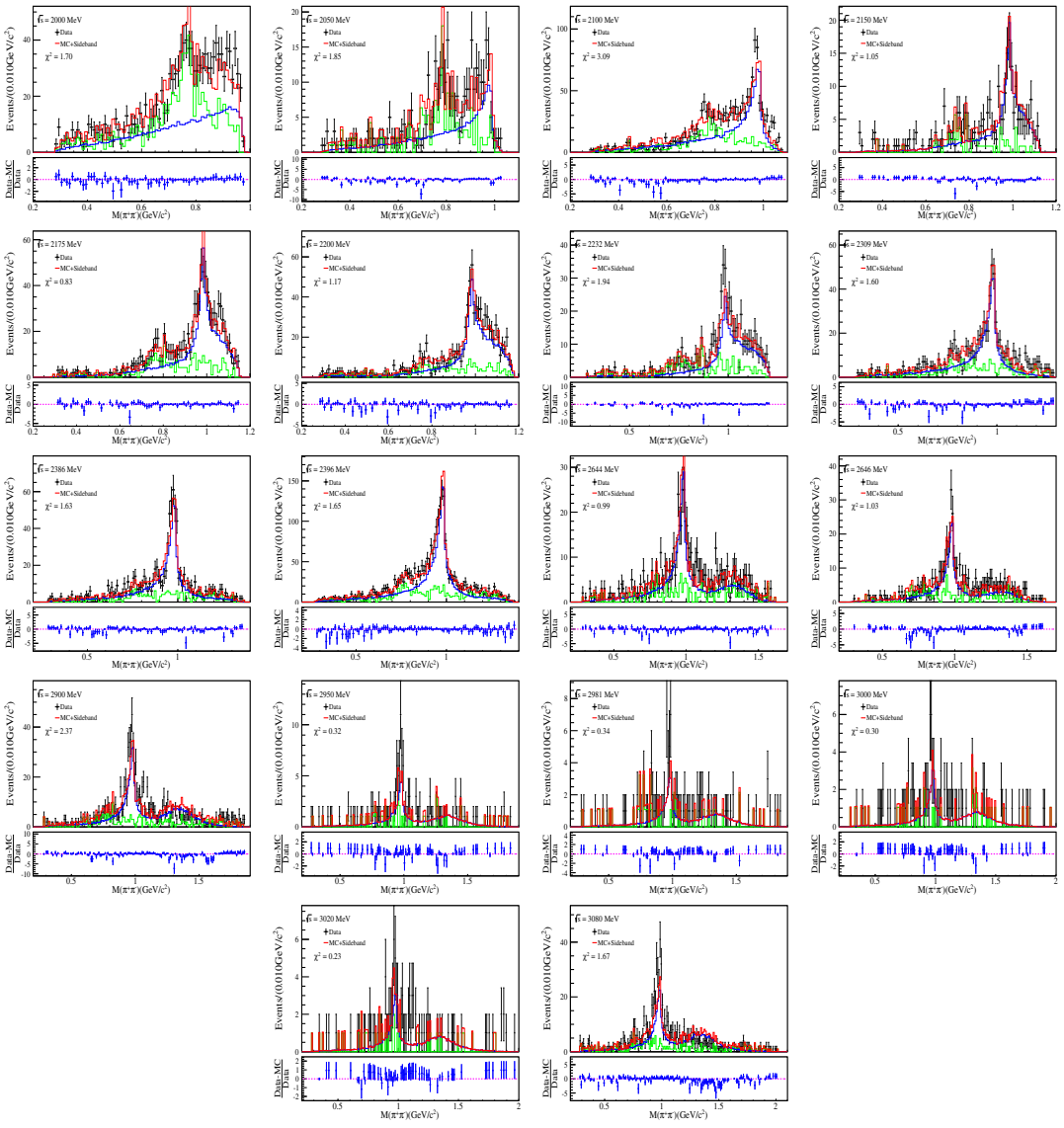

Figure 9: Comparison between Data and MC samples on M($\pi^+\pi^-$) distribution.

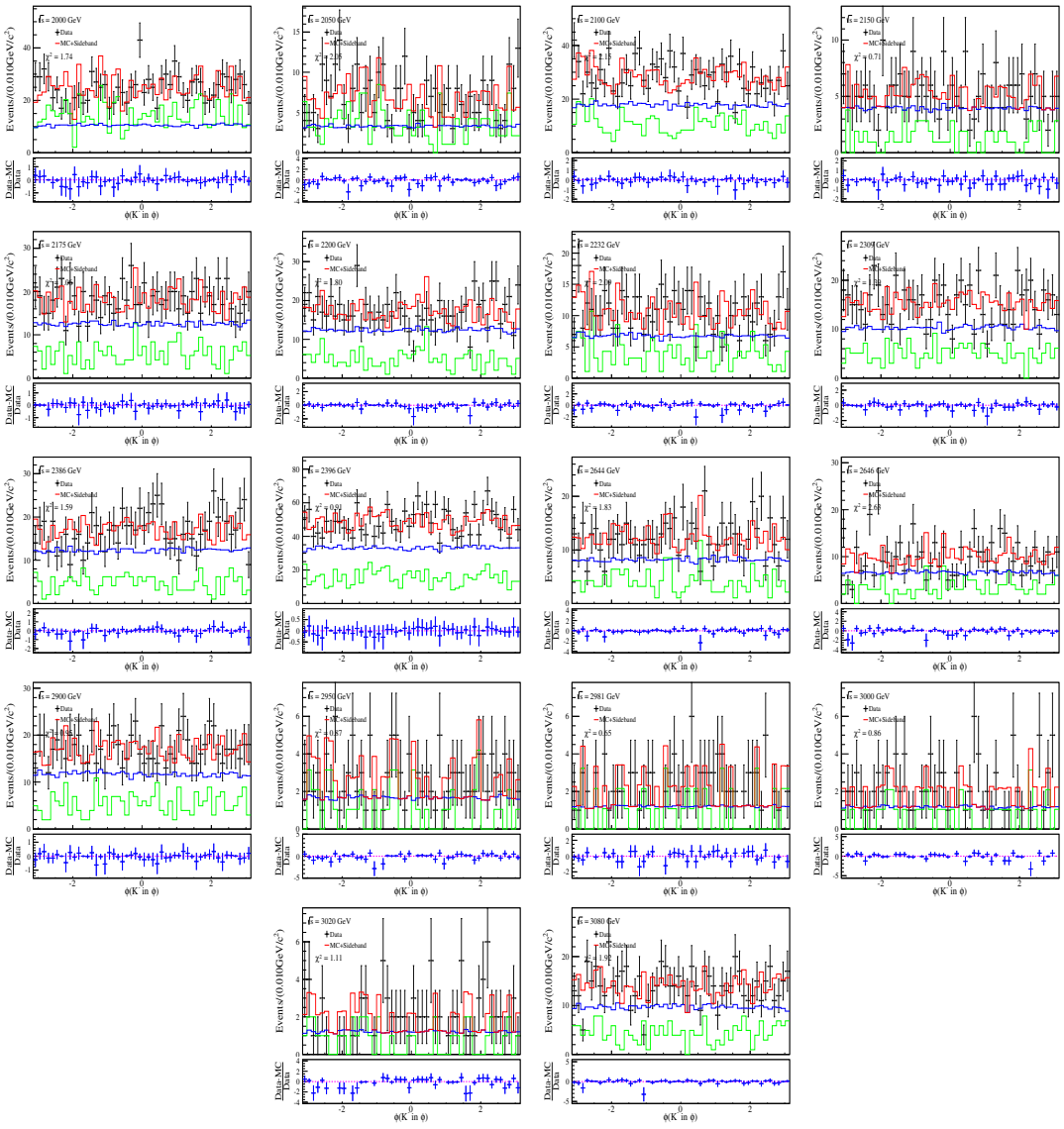

Figure 10: Comparison between Data and MC samples on ϕ angle distribution for K^- in CMS of ϕ particle.

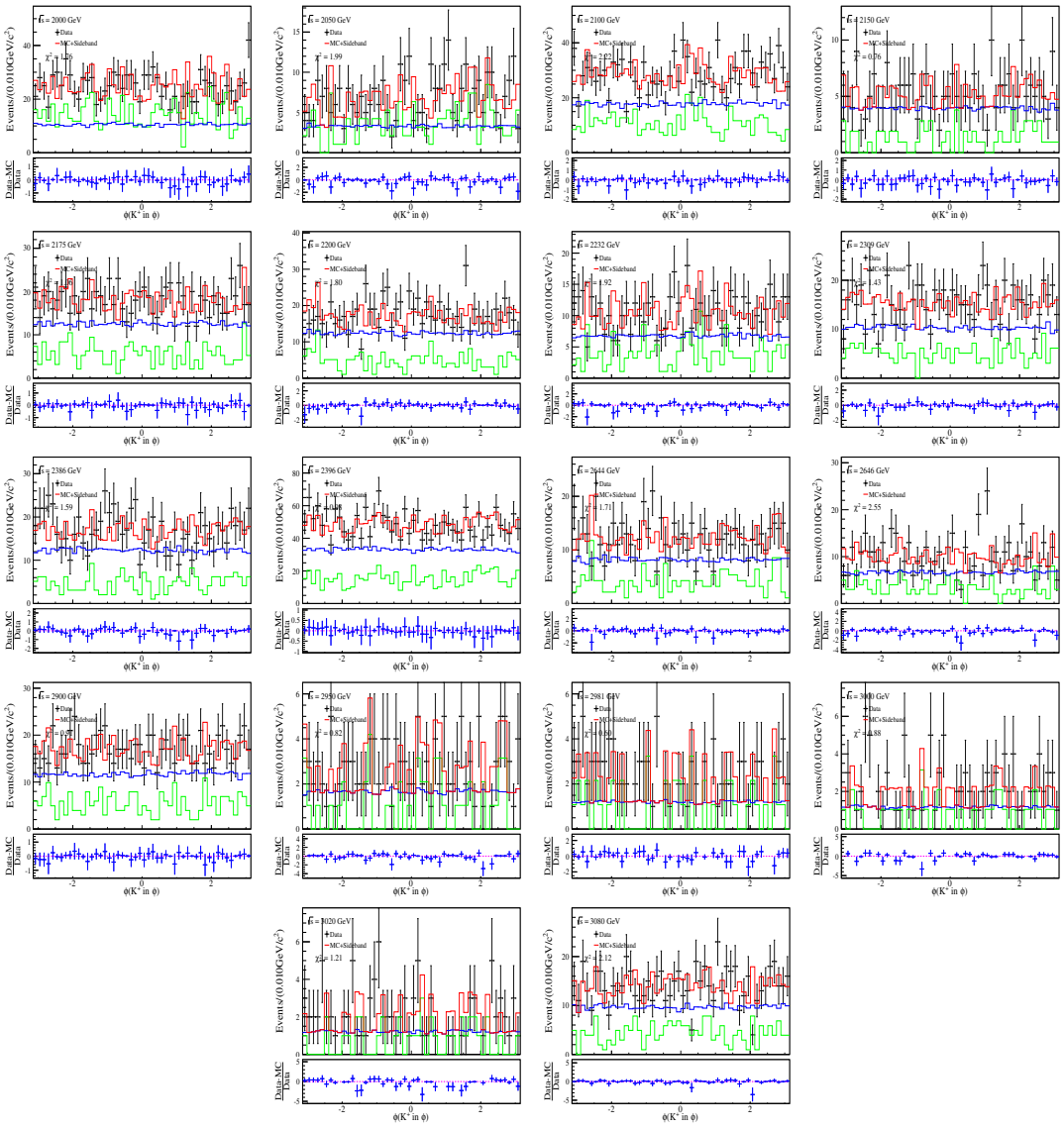

Figure 11: Comparison between Data and MC samples on ϕ angle distribution for K^+ in CMS of ϕ particle.

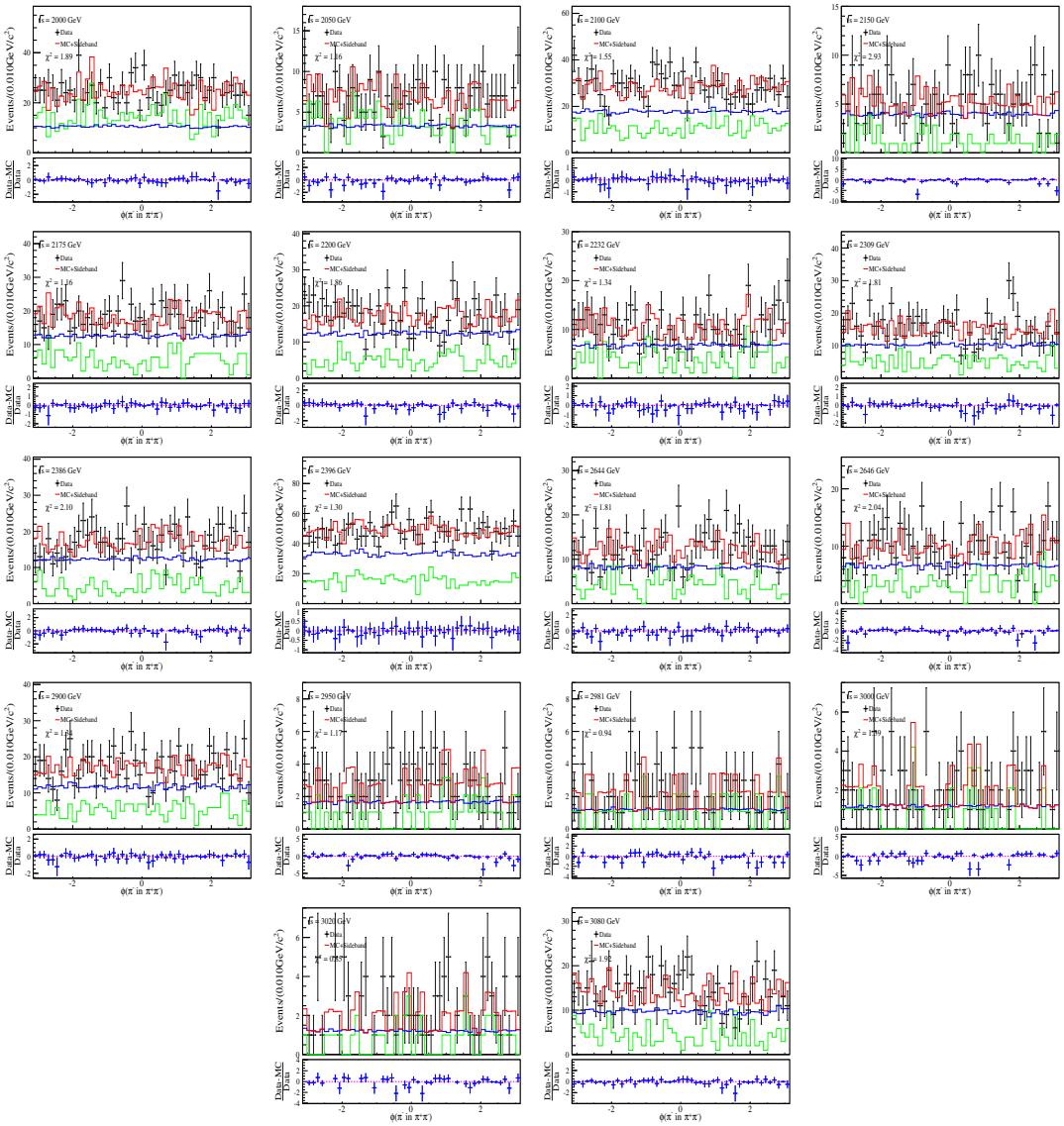

Figure 12: Comparison between Data and MC samples on ϕ angle distribution for π^- in CMS of $\pi^+\pi^-$.

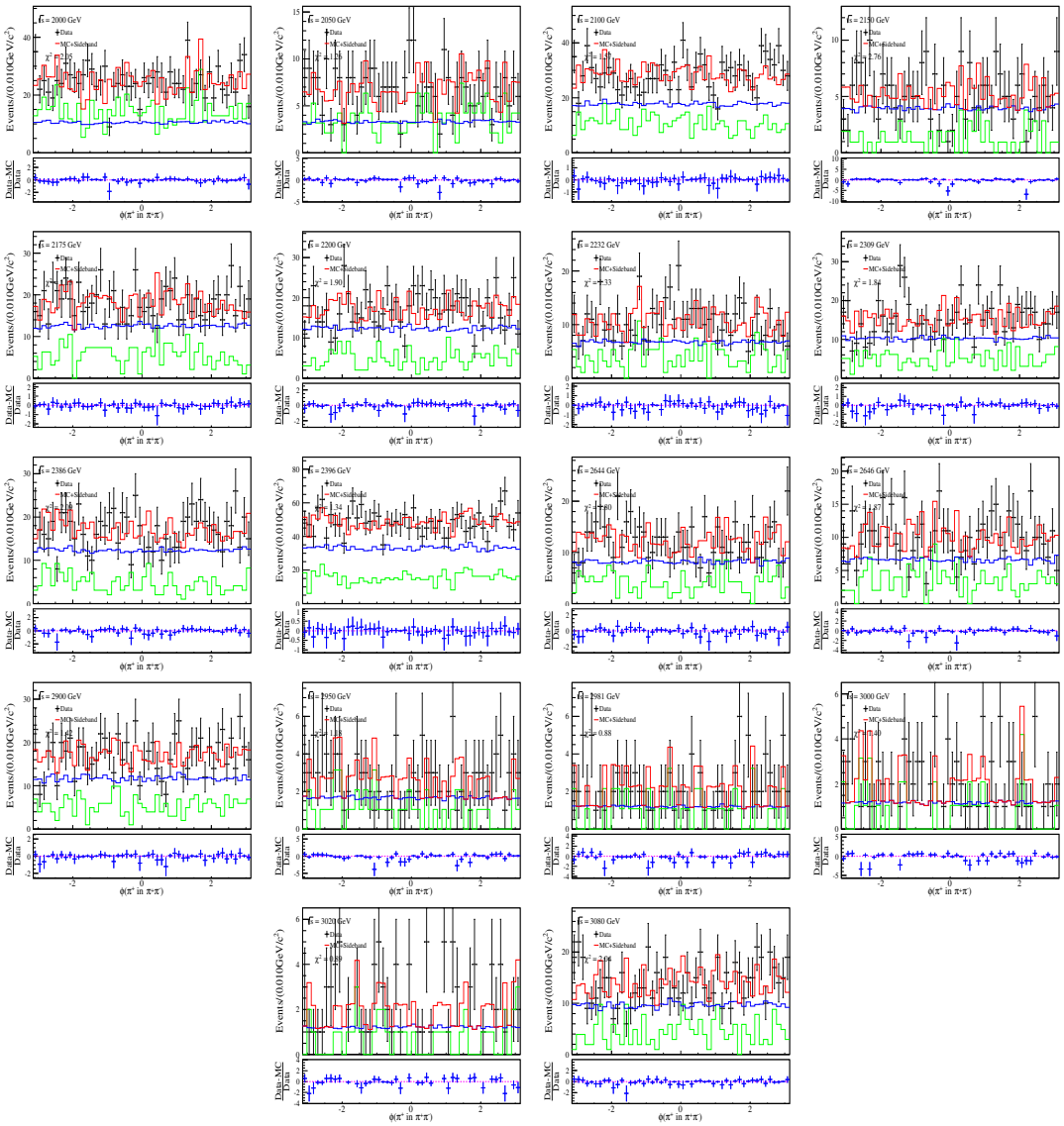

Figure 13: Comparison between Data and MC samples on ϕ angle distribution for π^+ in CMS of $\pi^+\pi^-$.

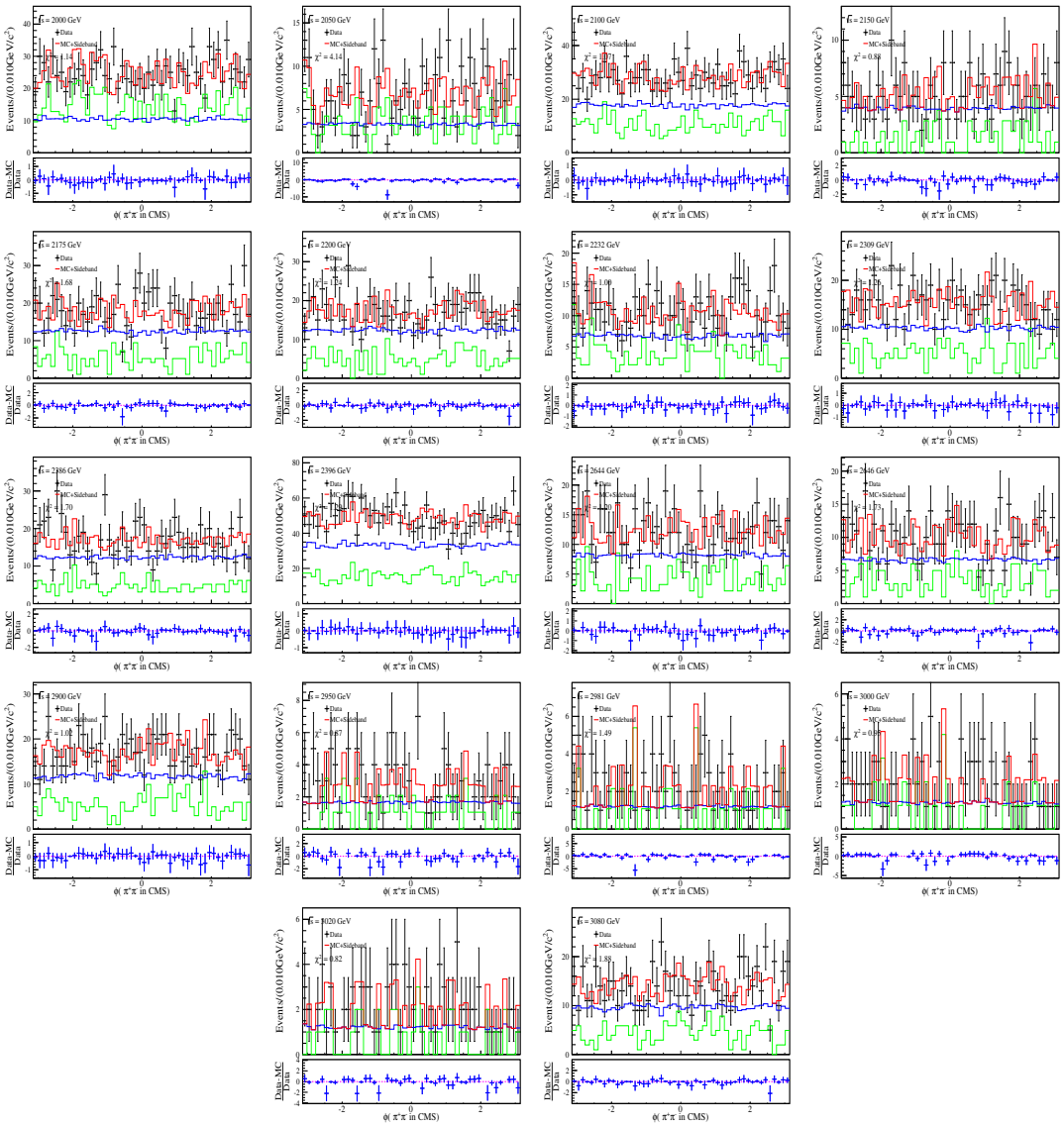

Figure 14: Comparison between Data and MC samples on ϕ angle distribution for $\pi^+\pi^-$ in CMS.

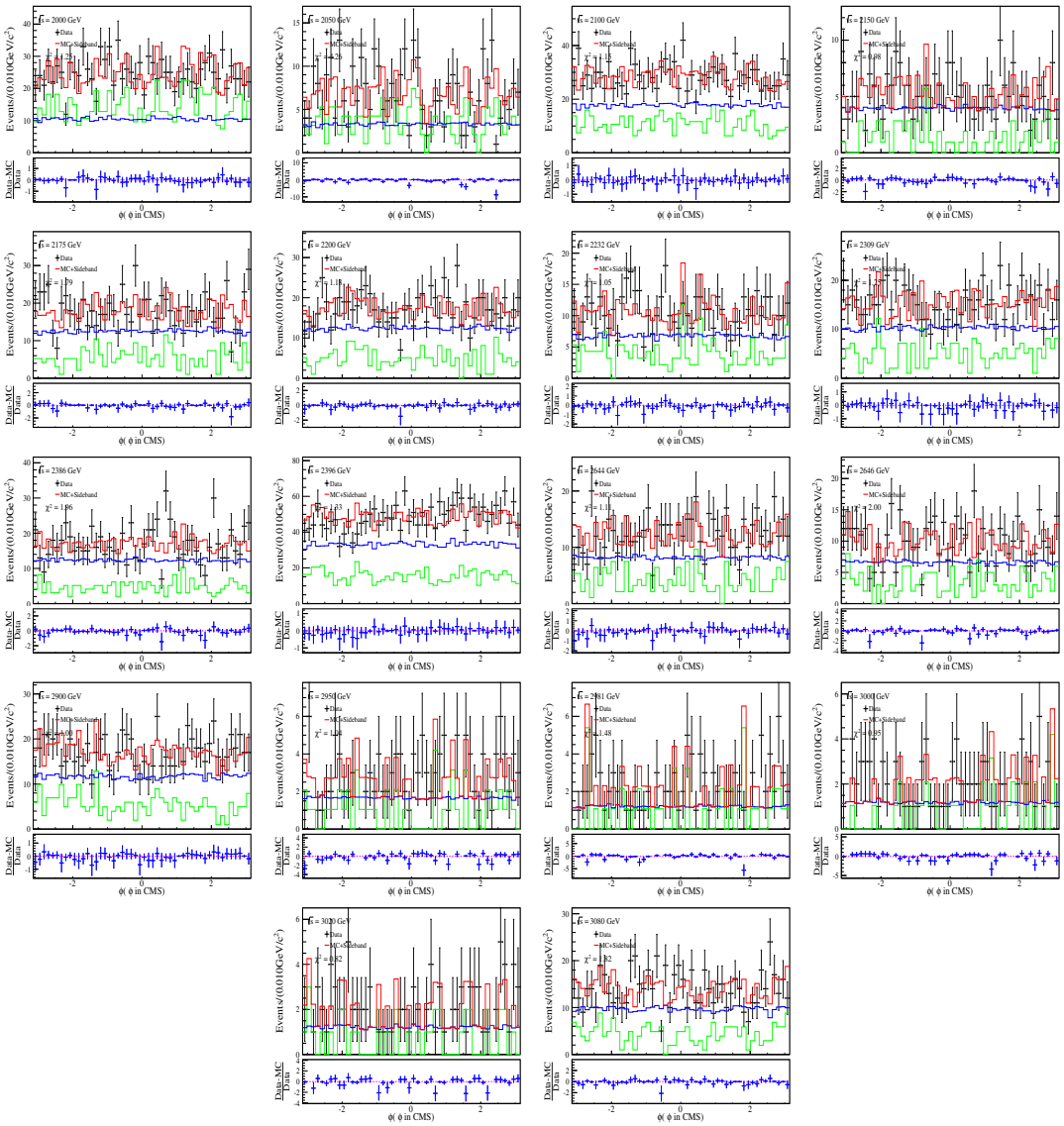

Figure 15: Comparison between Data and MC samples on ϕ angle distribution for ϕ in CMS.

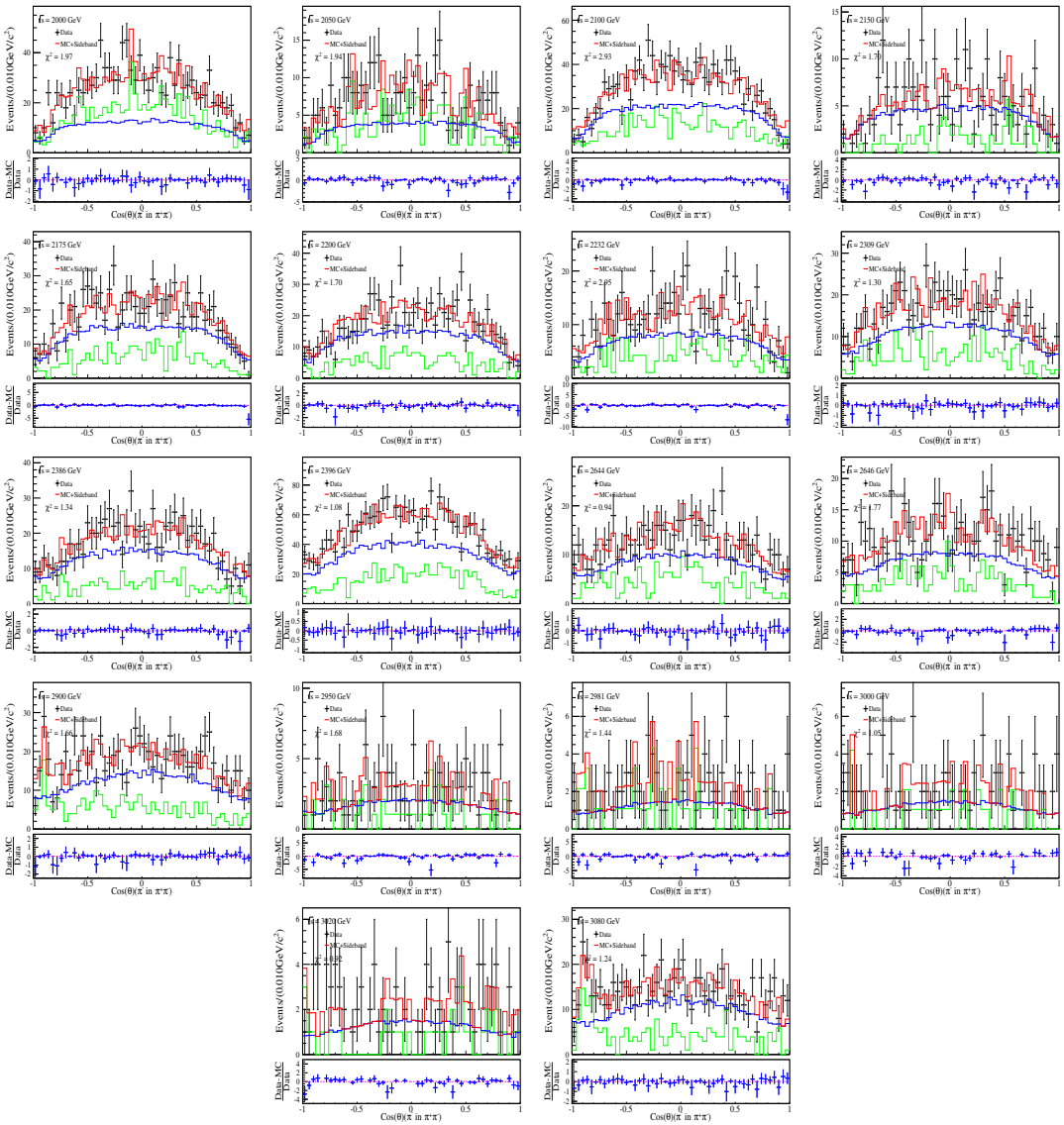

Figure 16: Comparison between Data and MC samples on Cos(θ) distribution for π^- in CMS of $\pi^+\pi^-$.

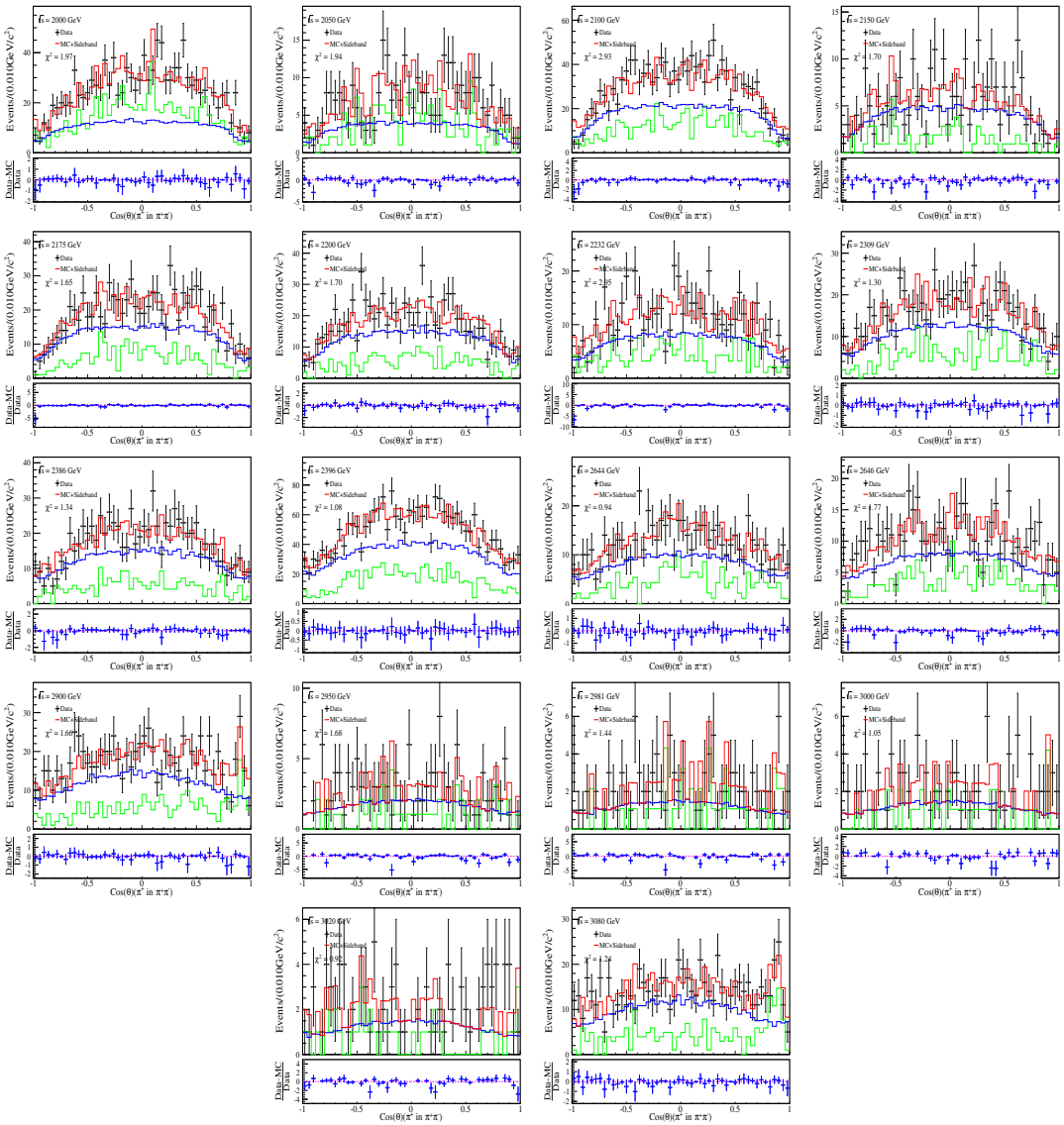

Figure 17: Comparison between Data and MC samples on Cos(θ) distribution for π^+ in CMS of $\pi^+\pi^-$.

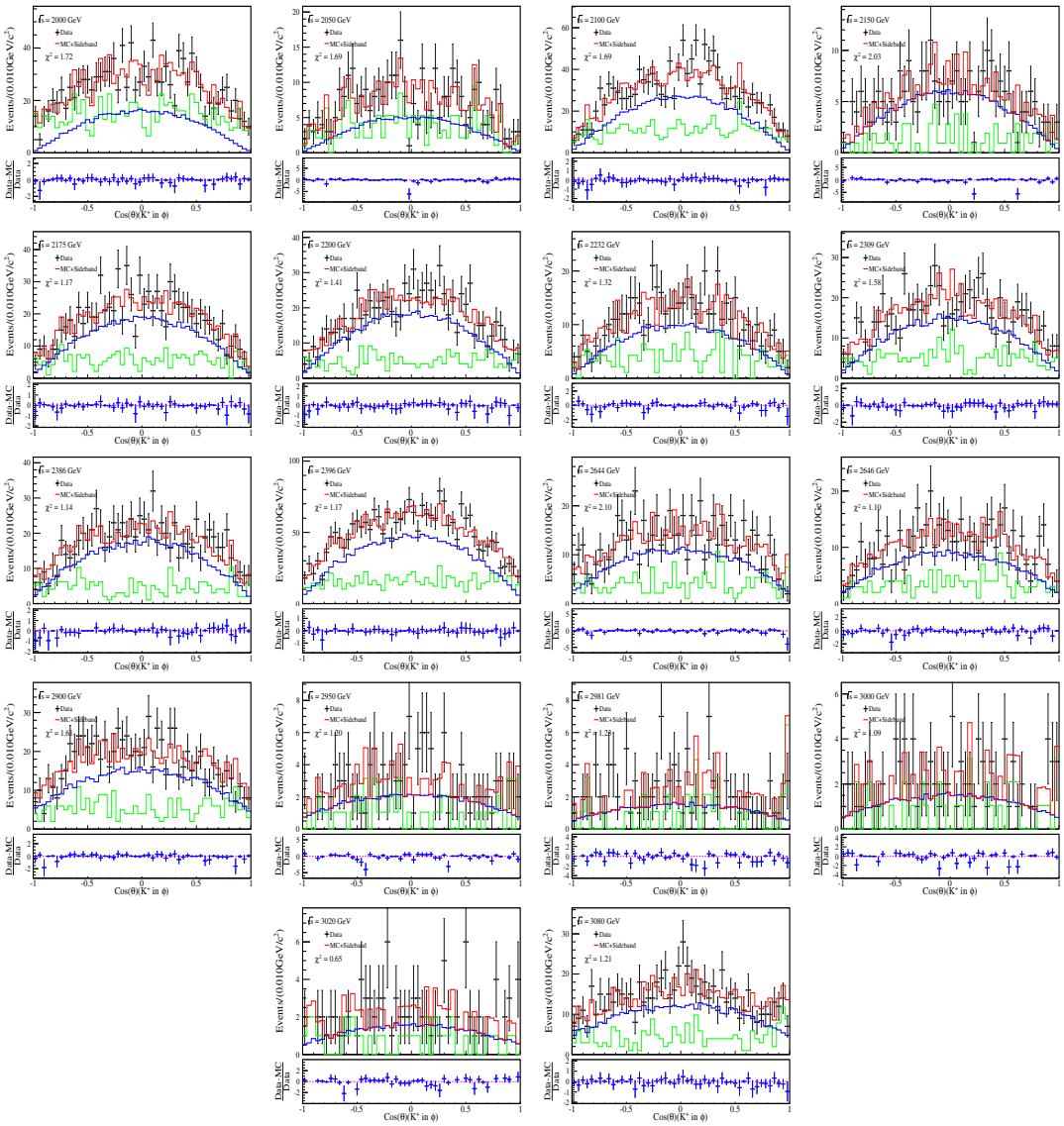

Figure 18: Comparison between Data and MC samples on Cos(θ) distribution for K^+ in CMS of ϕ.

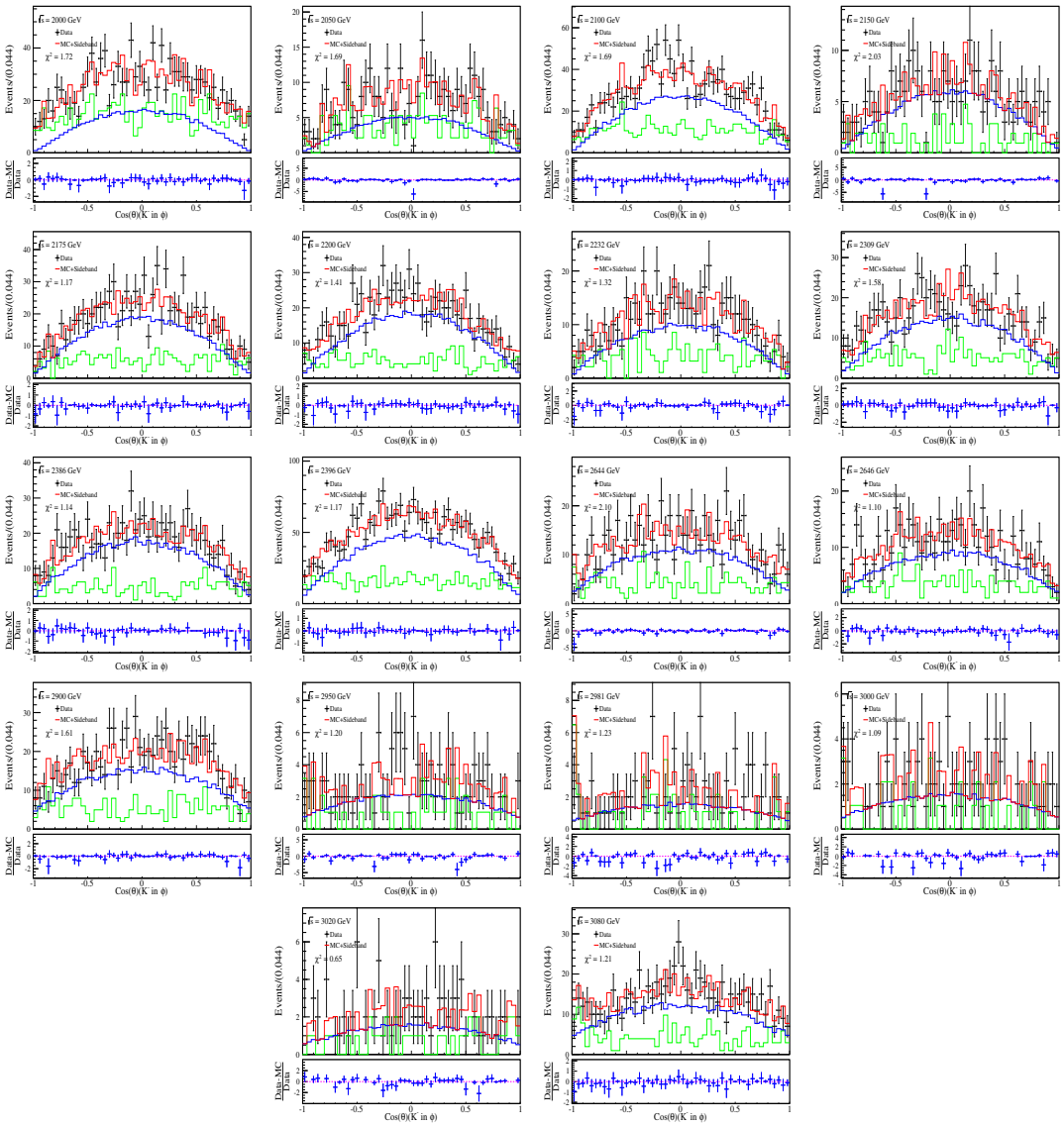

Figure 19: Comparison between Data and MC samples on Cos(θ) distribution for K^- in CMS of ϕ.

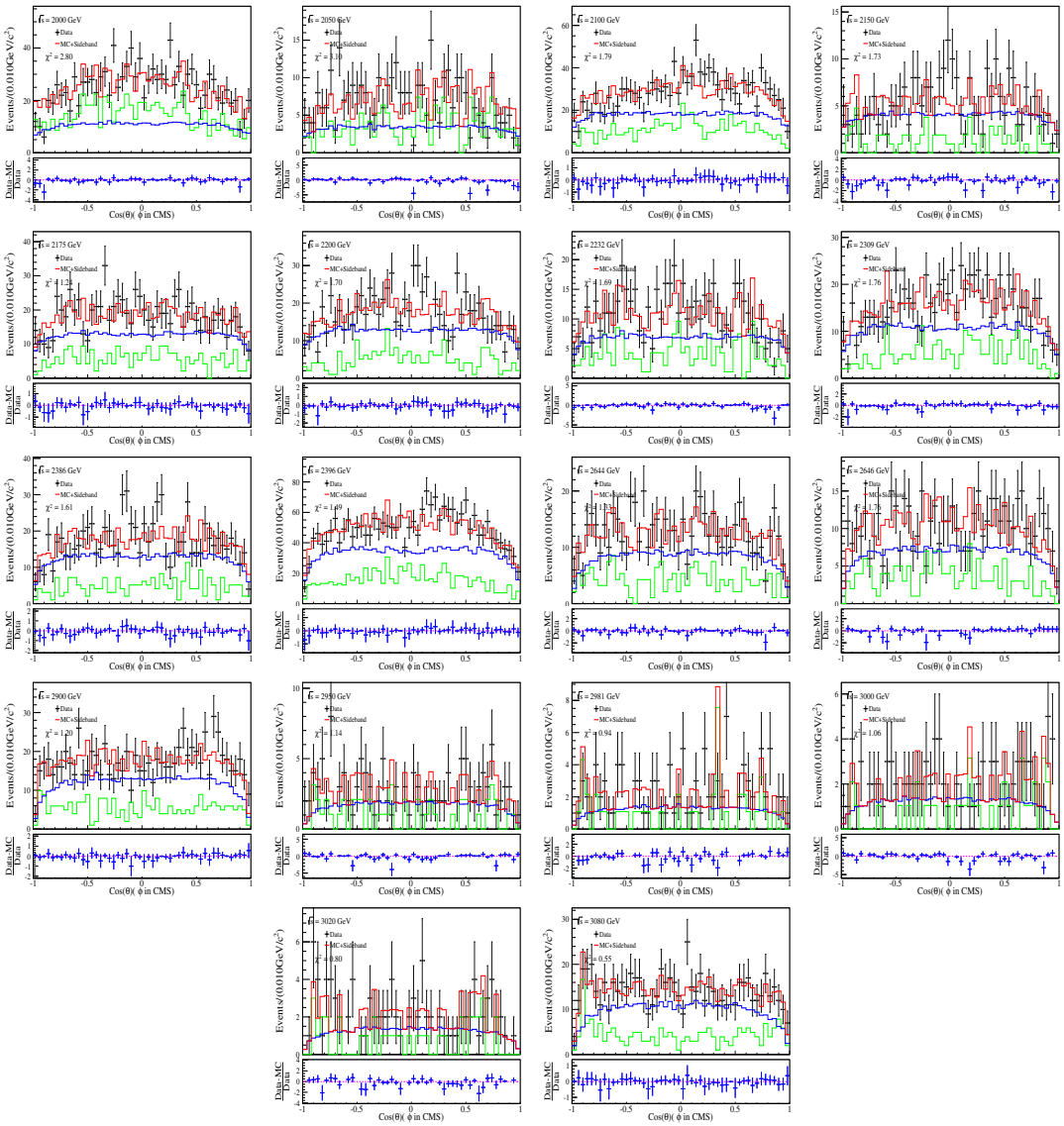

Figure 20: Comparison between Data and MC samples on Cos(θ) distribution for ϕ in CMS.

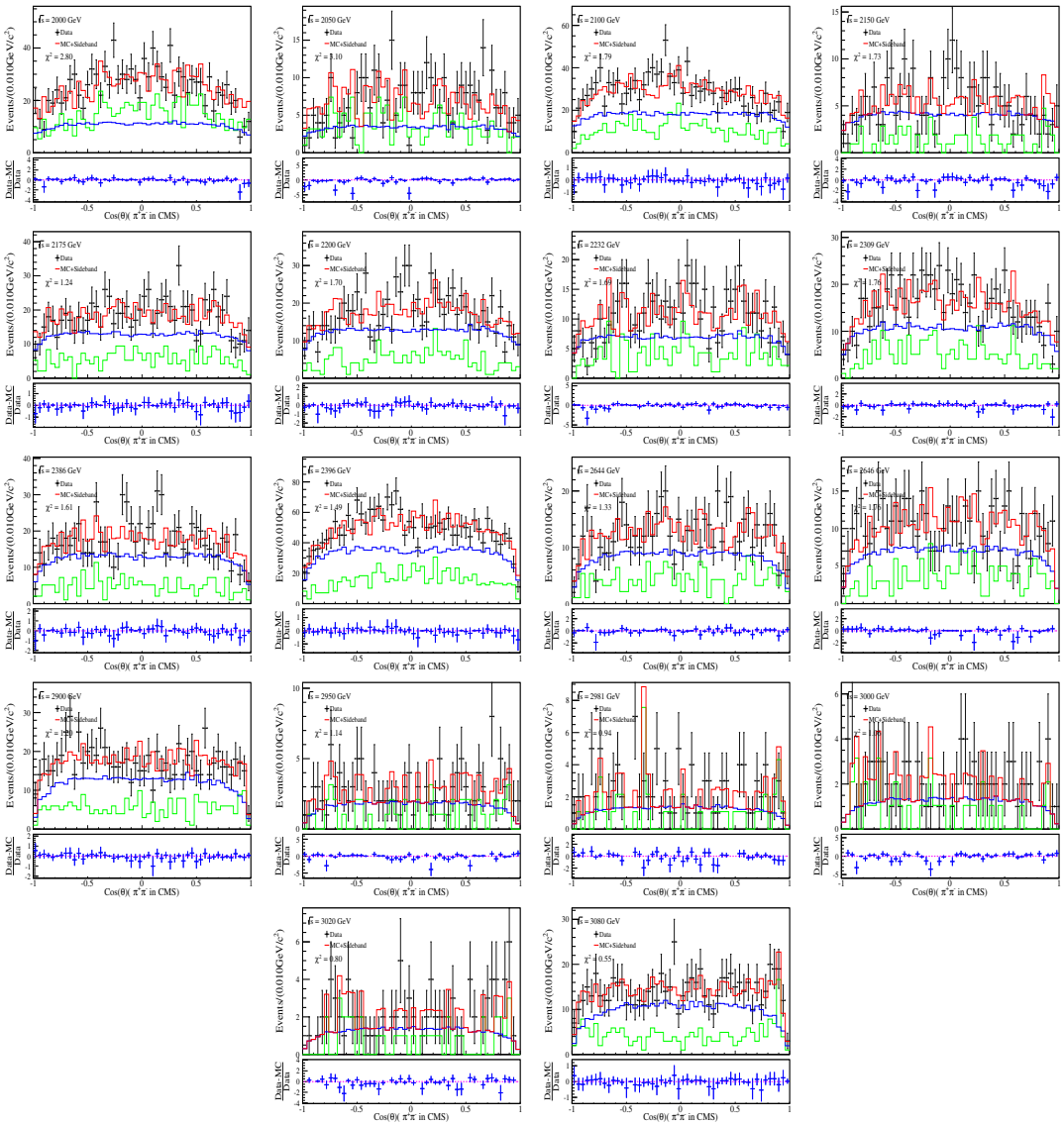

Figure 21: Comparison between Data and MC samples on Cos(θ) distribution for $\pi^+\pi^-$ in CMS.

$$\sigma e^+e^- \to \phi\pi^+\pi^- = \frac{N^{obs}}{\mathcal{L}_{int}\cdot(1+\delta^r)\cdot(1+\delta^v)\cdot\epsilon\cdot\mathcal{B}}, \quad (2)$$

where N^{obs} is the number of observed signal events, $\mathcal{L}_{int}$ is the integrated luminosity, $(1+\delta^r)$ is the ISR correction factor which is obtained by QED calculation and taking the line shape of the Born cross section measured by the BABAR experiment. $(1+\delta^v)$ is the vacuum polarization (VP) factor which is taken from QED calculation with an accuracy of 0.5%, ϵ is the detection efficiency including reconstruction and all selection criteria, $\mathcal{B}$ is the product branching ratio, $\mathcal{B}(\phi(1020) \to K^+K^-)$, taken from the Particle Data Group (PDG).

The final selection efficiency is measured according to MC simulation. The measured Born cross sections for $e^+e^- \to \phi(1020)\,\pi^+\pi^-$ at each energy point are listed in Table 4. Here the error is statistical only.

Table 4: Cross section of $e^+e^- \to \phi(1020)\pi^+\pi^-$.

$\sqrt{s}$ (GeV)	L (pb^{-1})	N(ϕ)	$(1+\delta)^{ISR}\times(1+\delta)^{VP}$	ϵ(%)	$\mathcal{B}$(%)	$\sigma(pb)$
3.080	126.19	576.9± 34.8	1.7387	0.2338	0.489	23.0± 1.4± 0.0
3.020	17.29	78.2± 12.2	1.7020	0.2656	0.489	20.5± 3.2± 0.0
3.000	15.88	74.6± 13.4	1.6901	0.2712	0.489	121.0± 3.8± 0.0
2.981	16.07	72.4± 15.2	1.6976	0.2788	0.489	19.5± 4.1± 0.0
2.950	15.94	114.4± 14.5	1.2333	0.3641	0.489	32.8± 4.2± 0.0
2.900	105.25	687.0± 37.7	1.3647	0.3427	0.489	28.6± 1.6± 0.0
2.646	34.00	423.4± 29.8	1.2480	0.3731	0.489	54.6± 3.8± 0.0
2.644	33.72	501.0± 33.2	1.2383	0.3793	0.489	64.6± 4.3± 0.0
2.396	66.87	1977.7± 65.5	1.1357	0.4062	0.489	131.8± 4.4± 0.0
2.386	22.55	697.3± 37.0	1.1239	0.4060	0.489	139.1± 7.4± 0.0
2.309	21.09	587.3± 37.7	1.2496	0.3674	0.489	124.0± 8.0± 0.0
2.232	11.86	435.2± 29.5	1.2609	0.3587	0.489	166.1± 11.2± 0.0
2.200	13.70	706.1± 38.3	1.1656	0.3818	0.489	238.0± 12.9± 0.0
2.175	10.62	760.8± 39.1	1.0032	0.4310	0.489	339.7± 17.5± 0.0
2.150	2.84	220.0± 20.0	1.0586	0.4002	0.489	372.9± 34.0± 0.0
2.125	108.49	9372.1± 144.1	1.0064	0.4053	0.489	431.6± 6.7± 0.0
2.100	12.17	1100.7± 51.1	1.0022	0.4048	0.489	457.0± 21.2± 0.0
2.050	3.34	191.5± 24.6	1.0604	0.3703	0.489	298.4± 38.3± 0.0
2.000	10.07	577.0± 46.8	1.0084	0.3682	0.489	315.0± 25.5± 0.0

5.4 Systematic error estimation

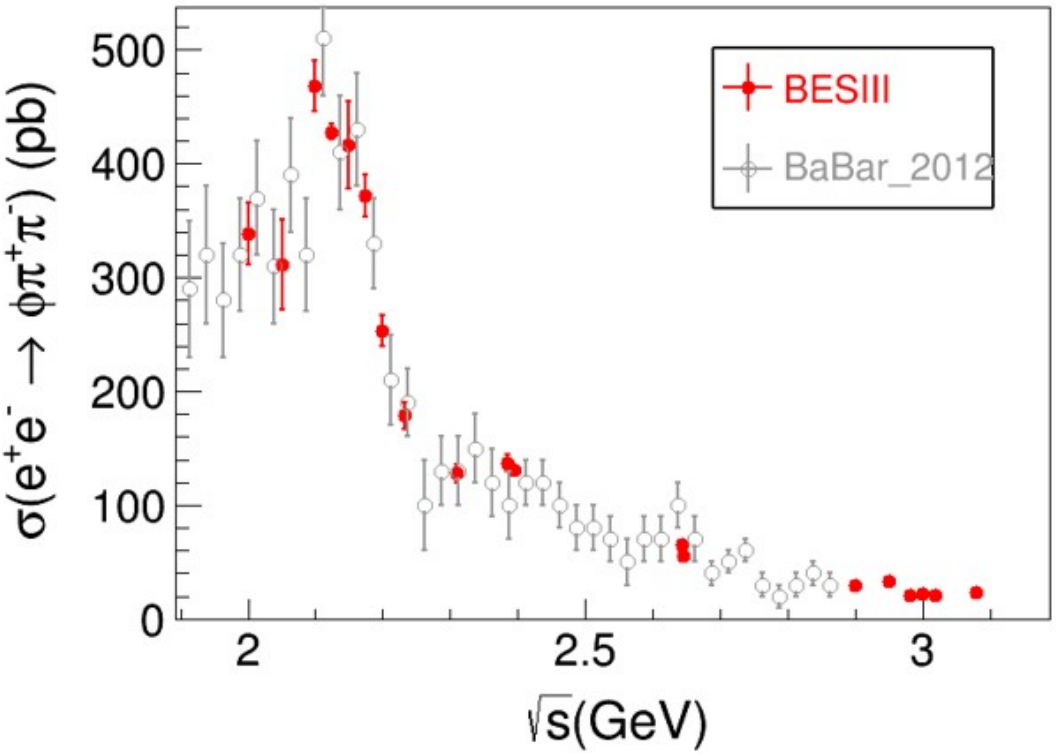

Figure 22: Cross section of $e^+e^- \to \phi(1020)\pi^+\pi^-$. The black dots with error bar are results from BABAR experiment. The red dots with error bar are results from this work.

Table 5: Systematic uncertainty of $e^+e^- \to \phi\,\pi^+\pi^-$ at 19 energy point.

$\sqrt{s}$ (GeV)	Lum	Tracking	PID	Kinematic	Sig shape	BG shape	ISR	ϕ Range	ISR	MC Statistic	Branch	Total
3.080	1.0	4.5	3.5	3.4	8.7	0.9	0.6	0.3	0.6	0.6	1.3	11.2
3.020	1.0	4.5	3.5	3.2	9.9	1.2	0.2	1.1	0.2	0.5	1.3	12.1
3.000	1.0	4.5	3.5	3.1	10.8	0.4	0.2	2.1	0.2	0.5	1.3	12.9
2.981	1.0	4.5	3.5	3.6	4.8	6.7	0.6	3.7	0.6	0.5	1.3	9.3
2.950	1.0	4.5	3.5	3.3	5.7	0.3	0.4	0.8	0.4	0.4	1.3	9.0
2.900	1.0	4.5	3.5	3.3	6.1	0.3	0.4	0.3	0.4	0.4	1.3	9.2
2.646	1.0	4.5	3.5	3.7	4.7	0.0	0.6	0.5	0.6	0.4	1.3	8.5
2.644	1.0	4.5	3.5	3.7	7.7	0.4	0.0	0.5	0.0	0.4	1.3	10.5
2.396	1.0	4.5	3.5	3.6	3.1	0.7	0.4	0.8	0.4	0.4	1.3	7.7
2.386	1.0	4.5	3.5	3.8	2.4	0.5	0.1	3.4	0.1	0.4	1.3	8.3
2.309	1.0	4.5	3.5	3.5	3.0	0.6	0.2	0.5	0.2	0.4	1.3	7.6
2.232	1.0	4.5	3.5	4.7	9.8	0.3	0.4	2.1	0.4	0.5	1.3	12.6
2.200	1.0	4.5	3.5	4.3	7.4	0.0	0.1	0.2	0.1	0.4	1.3	10.5
2.175	1.0	4.5	3.5	4.1	5.6	0.7	0.2	2.0	0.2	0.4	1.3	9.4
2.150	1.0	4.5	3.5	4.0	8.8	0.7	0.0	2.9	0.0	0.4	1.3	11.8
2.125	1.0	4.5	3.5	3.8	2.1	7.0	0.2	0.3	0.2	0.1	1.3	7.4
2.100	1.0	4.5	3.5	4.4	2.7	0.1	0.5	0.1	0.5	0.4	1.3	8.0
2.050	1.0	4.5	3.5	4.3	3.0	0.8	1.2	1.6	1.2	0.4	1.3	8.2
2.000	1.0	4.5	3.5	4.2	5.9	0.4	0.1	1.5	0.1	0.4	1.3	9.5

6 Structure in cross section line shape

A structure at $\sqrt{s} = 2.1$ GeV/c^2, corresponding to the so called $Y(2175)$, is observed in the cross section line shape of $e^+e^- \to \phi(1020)\,\pi^+\,\pi^-$. A fit to the line shape results in a mass of (2113 $\pm$ 5 $\pm$ 10) MeV/c^2 and a width of (108 $\pm$ 11 $\pm$ 10) MeV, where the first error is statistical and the second is systematic.

7 Summary

Based on the data sets collected with the BESIII detector at 19 center-of-mass energies from 2.0 to 3.08 GeV, the study of $e^+e^- \to \phi(1020)\ \pi^+\ \pi^-$ has been performed. We measured the cross sections with efficiency by PWA applied, a structure around $\sqrt{s} = 2.1$ GeV/c^2, corresponding to the so called $\phi(2170)$, is observed in the cross section line shape of $e^+e^- \to \phi(1020)\ \pi^+\ \pi^-$. A fit to the line shape results in a mass of (2113 $\pm$ 5 $\pm$ 10) MeV/c^2 and a width of (108 $\pm$ 11 $\pm$ 10) MeV, where the first error is statistical and the second is systematic.

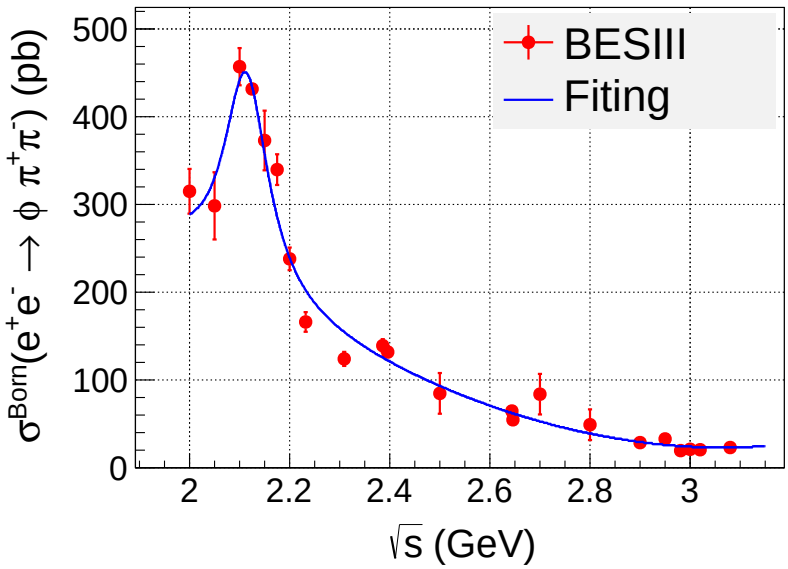

Figure 23: Cross section of $e^+e^- \to \phi(1020)\pi^+\pi^-$. The red dots with error bar are results of Cross Section measurement. The bule line is the fitting of cross section lineshape.

References

[1] B. Aubert *et al.* (BABAR Collaboration), Phys. Rev. D **74**, 091103(R) (2006);**76**, 012008(2007).

[2] M. Ablikim *et al.* (BES Collaboration), Phys. Rev. Lett.100, 102003 (2008).

[3] C.P. Shen *et al.* (Belle Collaboration), Phys. Rev. D **80**, 031101(R) (2009).

[4] M. Ablikim *et al.* (BESIII Collaboration), Phys. Rev. D **91**, 052017 (2015).

[5] M. Ablikim *et al.* (BESIII Collaboration), arXiv:1709.04323[hep-ex].

[6] G. J. Ding and M.L. Yan, Phys. Lett. B **650**, 390 (2007).

[7] G. J. Ding and M.L. Yan, Phys. Lett. B **657**, 49 (2007).

[8] X. Wang *et al.*, Phys. Rev. D **85**, 074024 (2012).

[9] S. S. Afonin and I. V. Pusenkov, Phys. Rev. D **90**, 094020 (2014).

[10] Z. G. Wang, Nucl. Phys. A **791**, 106 (2007).

[11] H. X. Chen *et al.*, Phys. Rev. D **78**, 034012 (2008).

[12] N. V. Drenska, R. Faccini and A. D. Polosa, Phys. Lett. B **669**, 160 (2008).

[13] L. Zhao *et al.*, Phys. Rev. D **87**, 054034 (2013).

[14] C. Deng *et al.*, Phys. Rev. D **88**, 074007 (2013).

[15] Yubing Dong *et al.*, Phys. Rev. D **96**, 074027 (2017).

[16] A. Martinez Torres *et al.*, Phys. Rev. D **78**, 074031 (2008).

[17] S. Gomez-Avila, M. Napsuciale and E.Oset, Phys. Rev. D **79**, 034018 (2009).

[18] M. Ablikim *et al.* (BESIII Collaboration), Nucl. Instrum. Meth. A **614**, 345 (2010).

[19] M. Ablikim *et al.* (BESIII Collaboration), Chinese Phys. C **41** 113001 (2017).

[20] B.S. Zou and D.V. Bugg, Phys. J. A **16** (2003) 537.

[21] B.S. Zou and D.V. Bugg, Phys. Rev. D **48**, R3948 (1993).

[22] S. M. Flatte, Phys. Lett. B **63**, 224 (1976).

[23] M. Ablikim *et al.* (BES Collaboration), Phys. Lett. B **607**, 243 (2005).

[24] M. Ablikim *et al.* (BES Collaboration), Phys. Lett. B **598**, 149 (2004).

[25] Z. H. Wang, reports in BESIII Physics and Software Workshop in Autumn of 2015 (http://indico.ihep.ac.cn/event/5099/session/12/contribution/38/material/slides/0.pdf)

[26] B. Hyams *et al.*, Nucl. Phys. B **64**, (1973) 134.

[27] S. Pislak *et al.*, Phys. Lett. B **87**, (2001) 221801.

[28] D. V.Bugg., Phys. Lett. B **572**, (2003) 1.

Appendices

A The Breit Wingner amplitudes for intermeidiate states.

The $f_0(980)$, $f_0(1370)$ *and* $f_2(1270)$ amplitudes and their parameters are taken from BESIIs previous analysis on $J/\psi \to \phi\pi\pi$ [23].

The $f_0(980)$ amplitude is described using the Flatte form:

$$f = \frac{1}{M^2 - s - i(g_1\rho_{\pi\pi} + g_2\rho_{KK})}, \tag{3}$$

Here ρ is Lorentz invariant phase space, $2k/\sqrt{s}$, where k refers to the π or K momentum in the rest frame of the resonance. The parameters of the Flatte formulae are determined accurately $M = 965 \pm 8(stat) \pm 6(syst)\ MeV/c^2$, $g1 = 165 \pm 10 \pm 15\ MeV/c^2$, $g2/g1 = 4.21 \pm 0.25 \pm 0.21$.

The $f_0(980)$ and f2(1270) amplitudes are described using constant Breit-winger formula:

$$f = \frac{1}{M^2 - s - iM\Gamma}, \tag{4}$$

where M and Γ are the corresponding mass and width, and are listed in Table 3. These parameters for $f_0(980)$, $f_0(1370)$ and $f_2(1270)$ are fixed in this analysis.

The σ amplitude and its parameters are taken from BESIIs previous analysis on $J/\psi \to \omega\pi\pi$ [24]. The form for the amplitude introduced by Zou and Bugg in fitting $\pi\pi$ elastic scattering data [21], consistent with Cern-Munich data on $\pi\pi$ elastic scattering[26] and with K_{e4} data[27], is used.

$$f = \frac{G_\sigma}{M^2 - s - iM\Gamma_{tot}(s)}, \tag{5}$$

$$\Gamma_{tot}(s) = g_1\frac{\rho_{\pi\pi}(s)}{\rho_{\pi\pi}(M^2)} + g_2\frac{\rho_{4\pi}(s)}{\rho_{4\pi}(M^2)}, \tag{6}$$

$$g_1 = f(s)\frac{s - m_\pi^2/2}{M^2 - m_\pi^2/2}exp[-(s - M^2)a]. \tag{7}$$

Here $\rho_{\pi\pi}$ is the usual $\pi\pi phase space 2k/\sqrt{s}$, and k is the momentum in the $\pi\pi$ rest frame. The form includes explicitly into $\Gamma(s)$ the Adler zero at s = $m_\pi^2/2$; the exponential factor cuts off the width at large s. A revised fit to $\pi\pi$ elastic data and K_{e4} using this formula is presented in [28]. In Eqn. 7,

$f(s) = b_1 + b_2 s$, where b_1 and b_2 are adjusted to reproduce the scattering length and effective range for $\pi\pi$ elastic scattering; these are from recent K_{e4} data of Pislak et al.[27]. In the second term of Eqn. 6, 4π phase space $\rho_{4\pi}(s)$ is approximated by $\sqrt{(1-16\mu^2/s)}/[1+exp(2.8-s)/3.5]$, with s in GeV^2. In practice, the 4π width is significant only at masses above 1200 MeV and has no effect on the σ pole. the optimum fit from BESIIs previous analysis [24] on $J/\psi \to \pi\pi$ is obtained with M = 0.9264, g_2 = 0.0024, a = 1.082, b_1 = 0.5843, b_2 = 1.6663 (all in units of GeV). These parameters are fixed in our analysis.

Table 6: Parameter of resonances in PWA fit.

Channel	Mass (MeV/c^2)	Width (MeV/c^2)
$f_0(980)$	965 ± 10	see in above
$f_0(1370)$	1350 ± 50	265 ± 40
$f_2(1270)$	1275 ± 15	190 ± 20
sigma	see in above	see in above

1 ‘